Geophysical Journal International

Geophys. J. Int. (2011) **186,** 82–98 doi: 10.1111/j.1365-246X.2011.05042.x

Crustal geophysics and seismicity in southern California

Egill Hauksson

Seismological Laboratory, Division of Geological and Planetary Sciences, California Institute of Technology, Pasadena CA, 91125*, USA.*
E-mail: hauksson@caltech.edu

Accepted 2011 April 9. Received 2011 March 10; in original form 2010 November 19

SUMMARY

The geographical distribution of the (1981–2005) seismicity in southern California forms a ±150 km broad zone adjacent to the Pacific–North America plate boundary, ranging from depths of ∼1–∼30 km, with the bulk of the focal depths in the range of 2–12 km. The distribution of the seismicity that includes both mainshock–aftershock sequences and background events is affected by both static and kinematic geophysical parameters of the crust. The static parameters include heat flow, topography, crustal density, V_p/V_s ratio, hypocentral fault-distance and crustal thickness from receiver functions. The tectonic loading is represented by kinematic parameters such as the crustal shear strain rate field, and the dilatational strain rate field. In our analysis, we normalize the seismicity relative to the areal density of the range of values of each of the parameters. Most of the seismicity occurs in areas of average heat flow, low to intermediate topography, average V_p/V_s and high late Quaternary fault density, and forms seismogenic zones that extend through the brittle crust. The location of late Quaternary faults, often described as zones of weakness, influences the geographical distribution of seismicity more than any other parameter. Although above or below average crustal properties such as high heat flow, thin crust or very low V_p/V_s values exist, these properties only influence the spatial distribution of seismicity in a minor way. As an example, the Salton Trough area of low topography, high heat flow, high V_p/V_s, high shear strain rate and thin crust has distributed seismicity within a thin seismogenic zone. Also, somewhat surprisingly, areas of high topography, low heat flow, low V_p/V_s, low shear strain rate and thick crust have low seismicity rates but a thin seismogenic zone. We determine an empirical relationship between heat flow and crustal thickness to show how the ∼400 °C temperature isotherm gradually deepens with crustal thickness and forms the base of the seismogenic zone for crustal thicknesses from 22 to 37 km. For crustal thickness ranging from 37 to 43 km, the ∼250 °C isotherm forms the base of the seismogenic zone, suggesting that seismic faulting in these regions is confined to the top of the upper crust (12–14 km), and thus does not accommodate plate motion.

Key words: Heat flow; Seismic cycle; Composition of the continental crust; Seismicity and tectonics; Continental tectonics: strike-slip and transform.

1 INTRODUCTION

Various static geophysical parameters have been determined for the southern California crust, including heat flow, topography, isostatic gravity, crustal average V_p/V_s, depth to Moho, and hypocentral fault-distance. In addition, kinematic crustal parameters such as shear strain rate, and dilatational strain rate from Global Positioning System (GPS) measurements, or as inferred from crustal and upper-mantle density modelling, are available. The spatial distribution of these parameters can be used to characterize regions of the crust most likely to have seismicity. Further, the depth distribution of seismicity provides insight into how these parameters may affect the thickness of the seismogenic zone. The lower limit of the seismogenic zone, presumably controlled by these parameters, has a sharp lower boundary, below which there are very few earthquakes and shear strains are likely accommodated by aseismic slip (e.g. Sibson 1982; Magistrale & Zhou 1996; Bonner *et al.* 2003).

The thickness of the seismogenic layer is a fundamental parameter for understanding earthquake physics and hazards analysis. Bonner *et al.* (2003) used the unrelocated southern California Seismic Network (SCSN) and NCSN catalogues, to argue that the thickness of the seismogenic layer in California is inversely related to heat flow, and that epicentral distributions tend to parallel thermal transitions. They identified two distinct ranges of temperature (dependent upon location) that describe the 99 per cent maximum depth of seismicity (D99) for California. These ranges are 450° ± 50 °C and 260° ± 50 °C, with the lower temperature range restricted to areas with heat flow below 50 mW m^{-2}. Bonner *et al.* (2003) also showed that for the 450 °C temperature region, the deep edge of the

envelope for the maximum energy released by earthquakes approximately coincides with the 400 °C isotherm.

Most previous studies have focused on analysing heat flow and seismicity. Using only heat flow, Tanaka & Ishikawa (2002) estimated the thermal structure beneath Japan and investigated the thermal influence on maximum seismicity depth in the crust. They found that the 90 per cent maximum depth of seismicity range (D90) was between 200 °C and 500 °C. They argued that the consistency of temperature for D90 over a large depth interval implied that temperature is the dominant factor controlling maximum depth of seismicity. Similarly, Doser & Kanamori (1986) analysed the depth of seismicity in Imperial Valley, California. They showed that regional variations in focal depth were related to heat flow and in some cases to variations in crustal structure. In a regional Western US study, Wong & Chapman (1990) analysed heat flow and deep earthquakes to show that crustal and upper mantle temperatures could be anomalously low where earthquakes occur below the normal crustal seismogenic zone. Using a damage rheology model Ben-Zion & Lyakhovsky (2006) showed that productivity of earthquakes is inversely correlated with heat flow derived temperature and sediment cover thickness. Thus temperature seems to play a major role in defining the seismogenic crust.

The shear deformation caused by the Pacific and North America Plate motion is localized along the principal slip surfaces (PSZs) of the late Quaternary faults (Fig. 1), which form a ∼300 km wide northwest striking region of crustal deformation across southern California (Tape *et al.* 2009). The late Quaternary faults are often described as zones of crustal weakness (e.g. Carena & Moder 2009). The major earthquakes occur along the PSZs but the background seismicity rate decays away from each of the PSZs, forming a broad zone of crustal deformation (Hauksson 2010). Each year, about 14 000 earthquakes of M > 1.0 are recorded by the SCSN (Hutton *et al*. 2010). These earthquakes are unevenly distributed within the southern California crust, and occur as mainshock–aftershock sequences or swarms (Vidale & Shearer 2006). The availability of high-precision earthquake locations (Lin *et al.* 2007) makes it possible to measure precisely the distances between the individual hypocentres and the PSZs. The distribution of these measurements shows that the background seismicity is located near the PSZs (Hauksson 2010).

Previously, Nazareth & Hauksson (2004) used relocated seismicity and finite source models for large earthquakes to determine the seismogenic thickness of the southern California crust. They found regional variations from 5 to 25 km depth in the depth of the seismogenic zone. We build on their study by performing a more general analysis of the geophysical properties of the southern California crust. We study the depth distribution of seismicity for each of the geophysical parameters to determine what values of each of the parameters have the strongest influence on the depth of the seismogenic zone.

To avoid biases caused by the values of a certain geophysical parameter being too common or too rare, we normalize the seismicity relative to the range of available parameter values. First, we determine relative histograms of each of the parameters at each hypocentre and the corresponding parameter sampled on an evenly spaced grid. Secondly, we determine the relative ratio of these histograms to identify higher or lower than average seismicity rates.

In this study, we use the waveform relocated background seismicity (1981–2005) and the geophysical crustal properties to improve our understanding of the seismogenic zone beneath southern California. We determine if earthquakes occur more commonly within crustal volumes characterized by certain values of the geophysical parameters. In particular, we use the heat flow and crustal thickness data to infer the effects of temperature on the depth distribution of seismicity. Further, we explore if some range of values of the geophysical crustal properties are more likely to accommodate earthquakes than others.

2 DATA PROCESSING

The study area includes most of southern California where the SCSN coverage has a magnitude of completeness (M_c) of 1.8. We analysed the version of the SCSN earthquake catalogue that was relocated by Lin *et al.* (2007). They also published a SCSN station map, which is a proxy for the spatial distribution of the hypocentral uncertainties. We included only earthquakes with well-constrained hypocentres by applying the following selection criteria of horizontal error of less than 1 km, vertical error less than 2 km, root-mean-square (rms) error less than 0.6 s and the distance to the closest station of 30 km or less. We also filter the catalogue to exclude events of $M < 1.8$.

The data for each of the geophysical parameters are selected from the geographical area as outlined by the polygon in Fig. 2(a). We determine a set of values of each of the geophysical parameters by sampling on a regular grid of 0.01°, which matches approximately the uncertainty of ∼1 km in the hypocentral parameters (Lin *et al*. 2007). Similarly, we determine the value of a geophysical parameter, such as heat flow at the epicentre of each earthquake, by using surface fitting interpolation (Wessel & Smith 1998).

As described in the Appendix, we determine normalized histograms of values for both a parameter at each hypocentre and the same parameter sampled on a regular grid. These are shown as black and red curves in Figs 2(c) to 10(c). We divide the two normalized histograms (divide black by red) to obtain the ratio of earthquakes per unit of the chosen geophysical parameter (shown as the curve with red dots in Figs 2d–10d).

If the ratio of seismicity per unit of a parameter exceeds 1.0 the rate of seismicity is considered to be greater than average, and if the value is less than 1.0 the rate of seismicity is less than average. As an example, in the case of heat flow the two histograms of the heat flow values at epicentres and the heat flow values on a regular grid show that the seismicity rate is higher than average in the range from 50 to 100 mW m^{-2} and lower than average for 100 mW m^{-2} or larger heat flow (Figs 2c and d). The relative cumulative plot in Fig. 2(d) shows within what range of a parameter the seismicity is most common.

3 RESULTS

We group heat flow, topography, crustal density, V_p/V_s, crustal thickness, hypocentral fault-distance as static crustal parameters because they quantify the long-term properties of the crust. The hypocentral fault-distance measurements differ from the other geophysical parameters because they depend on the seismicity patterns from 1981 to 2005. Seismicity patterns can remain mostly unchanged for long periods of time. However, major mainshock–aftershock sequences can produce large spatial and temporal variations in the seismicity (e.g. Ben-Zion 2008). If we presume that the 1981–2005 seismicity patterns are a representative sample, the distribution of fault-distance measurements should remain similar with time. In contrast, we group the shear strain, dilatational strain and the model

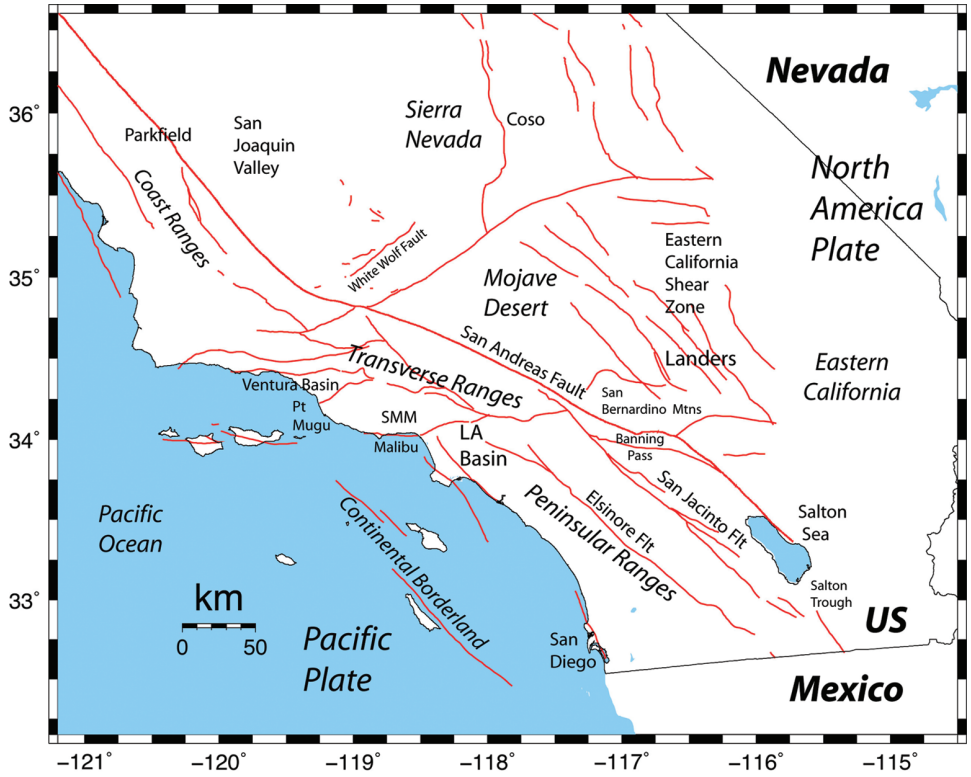

Figure 1. Map showing the locations of major geographical and tectonic features in southern California.

crustal dilatation as kinematic parameters describing steady-state deformation of the crust. We analyse these parameters to determine how they relate to the spatial distribution of southern California seismicity and the depth extent of the seismogenic zone.

3.1 Static crustal parameters

The static crustal parameters describe properties of the crust that can be measured with a variety of geophysical techniques. These properties have been in place for much longer period of time than the crustal strain rate properties that are mostly based on GPS data.

3.1.1 Heat flow

The geographical variations in heat flow and the spatial density of earthquakes form heterogeneous distributions across southern California (Fig. 2a). We analysed the extensive heat flow data set, available from http://smu.edu/geothermal/ (see also, Bonner *et al.* 2003) and the waveform relocated earthquake catalogue from Lin *et al.* (2007). The regions of low heat flow include the central Peninsular Ranges, southwestern Mojave, Ventura Basin and southern Sierra Nevada. The regions of high heat flow include the Salton Trough, areas offshore from San Diego, parts of the eastern Mojave Desert and Coso geothermal area. The seismicity forms a heterogeneous spatial distribution across these regions, with most of the seismicity in areas of average heat flow.

The plot of heat flow values at each of the epicentres and the corresponding focal depths shows that most of the earthquakes occur in the average heat flow regime from 55 to 110 mW m^{-2} (Fig. 2b). We arbitrarily colour code the low heat flow values blue ($\leq$55 mW m^{-2}), average heat flow values green (55–110 mW m^{-2}) and high heat flow values red ($\geq$110 mW m^{-2}). At very low heat flow values of less than 55 mW m^{-2}, below the high Sierras and parts of the Peninsular Ranges, there are a few clusters of hypocentres scattered at shallow depth. Approximately 85 per cent of the seismicity occurs in the areas with average heat flow values, between heat flow of 55 and 110 mW m^{-2}. The seismicity associated with high heat flow values of greater than 110 mW m^{-2} exhibits a prominent decrease in the depth of earthquakes with increasing heat flow. Most of this seismicity is located within geographically limited geothermal areas of high heat flow.

The maximum depth of 95 per cent of the seismicity (D95) exhibits increasing depth between 50 and 100 mW m^{-2} but decreasing depth for higher heat flow values. The complex pattern of focal depths versus heat flow suggests that factors other than just heat flow alone affect the thickness of the seismogenic zone as well as the preferential geographical distribution of earthquakes.

The normalized histograms of evenly sampled heat flow values and heat flow values at epicentres exhibit a similar distribution, with most of the values in the range from 30 to 160 mW m^{-2} (Fig. 2c). The ratio of number of heat flow values at epicentres and the corresponding number of heat-flow-grid values shows that the number of earthquakes is more than average in the range from 50 to 100 mW m^{-2} (Fig. 2d). The ratio of the two histograms shows that the above average seismicity rate in the average heat flow range is significant. The above average occurrence of seismicity in areas with average heat flow suggests that the geographical distribution of seismicity is influenced more strongly by other factors than heat flow. In contrast, Enescu *et al*. (2009) and Yang & Ben-Zion (2009) showed that the temporal behaviour of seismicity is strongly influenced by heat flow.

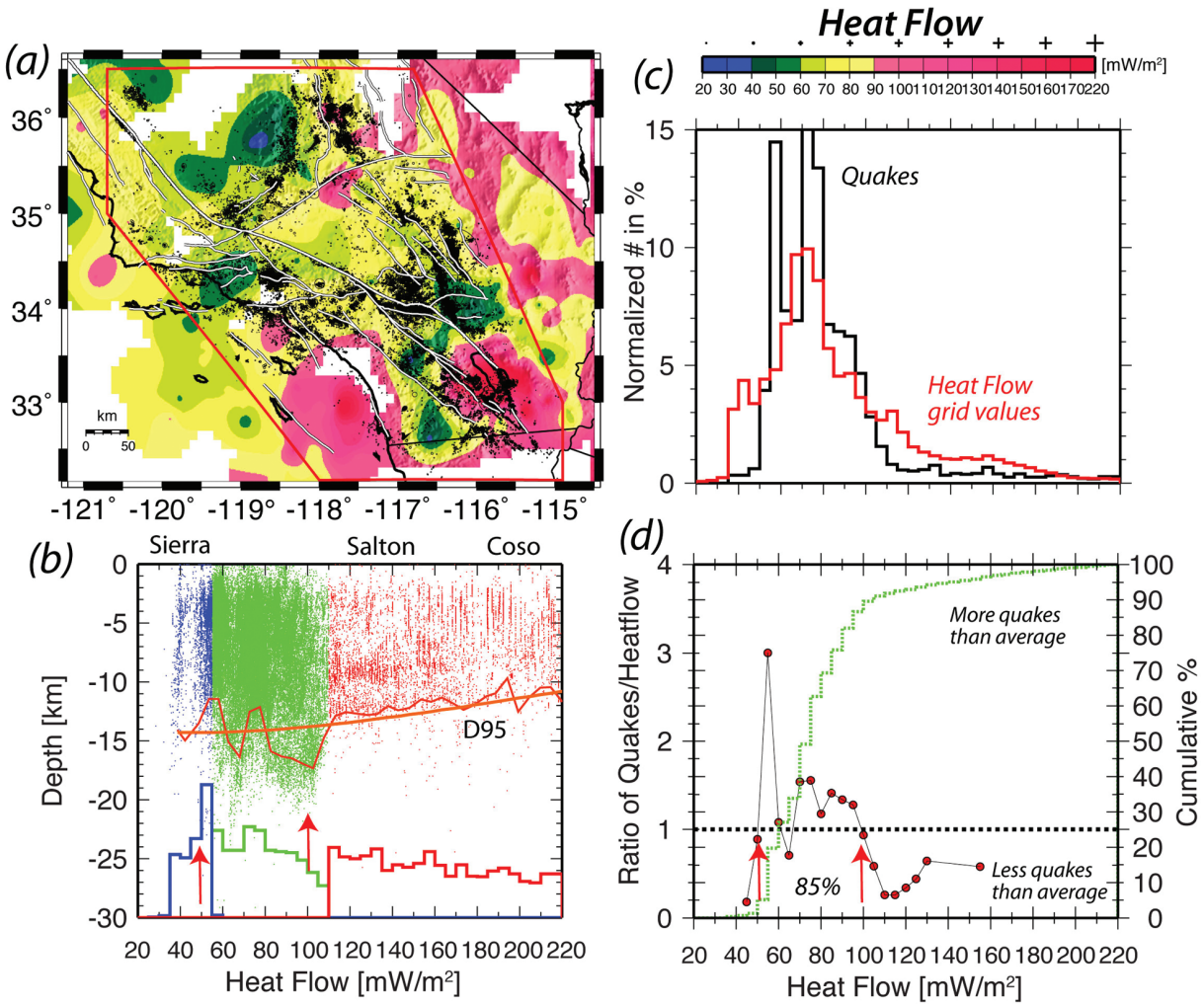

Figure 2. Heat flow and seismicity. (a) Earthquakes of $M \geq 1.8$ are plotted on top of the heat flow for southern California within the study area outlined by the red polygon. (b) Each hypocentre is plotted at the respective focal depth and heat flow value interpolated from the map. Detailed and smooth versions of the 95 per cent maximum seismicity depth contour are plotted in orange colour. (Bottom) histograms separating the three ranges of heat flow values, 0–55 (blue), 55–110 (green) and 110–3000 (red) mW m^{-2}, with $y = \log10(1.0 +$ frequency percent) with full scale of 5.0. (c) Normalized histograms of quakes and 'heat flow values' for each 10 (mW m^{-2}) interval of heat flow. The abscissa is the same as in panel (d). (d) Ratio of the two histograms in (c) per 10 (mW m^{-2}) interval in heat flow (curve with red dots) and cumulative number of quakes (green curve). The arrows indicate the range of heat flow where the percent (value shown in plot) of the seismicity occurs.

3.1.2 Topography

We used 30-s topographic data from the USGS (GTOPO30) and determine the elevation at each epicentre in the catalogue. The topography where earthquakes occur varies from about –70 to 3500 m relative to sea level in southern California (Fig. 3a). The lowest topography exists offshore, in the Salton Trough, San Joaquin Valley and parts of eastern California. The highest topography is found in the Sierra Nevada, with somewhat lower but elevated topography in mountain ranges such as the Transverse Ranges and the Peninsular Ranges.

The seismicity is distributed unevenly over all elevation ranges. The plot of the focal depth distribution of earthquakes versus topographic elevation at each epicentre shows that earthquakes are common at sea level up to 2000 m, with a decrease in both focal depths and the number of events at higher elevations (>1600 m) (Fig. 3b). The 95 per cent maximum focal depths show shallow focal depths at less than 100 m elevation and at elevations above ∼2000 m. The high heat flow events in the Salton Trough and Coso geothermal area occur at ∼0 m and 1100 m elevations, respectively.

The normalized histograms of evenly sampled elevation values and elevation values at epicentres exhibit different distributions, with low elevation values being very common and earthquakes being apparently more common above 600 m (Fig. 3c). The ratio of the number of heat flow values at epicentres, and the corresponding number of elevation grid values shows that more earthquakes than average occur above 600 m elevation (Fig. 3d). In regions above 2000 m elevation, there is little seismicity and very small fraction of southern California has such high topography, and the ratio is not meaningful. The ratio of elevation values and the cumulative distribution of epicentres show that 40 per cent of the seismicity occurs at elevations below 600 m and that 55 per cent of the seismicity occurs in the elevation range from 600 m up to 2000 m (Fig. 3d). Thus topography does not seem to have a significant unexpected correlation with the spatial distribution of seismicity.

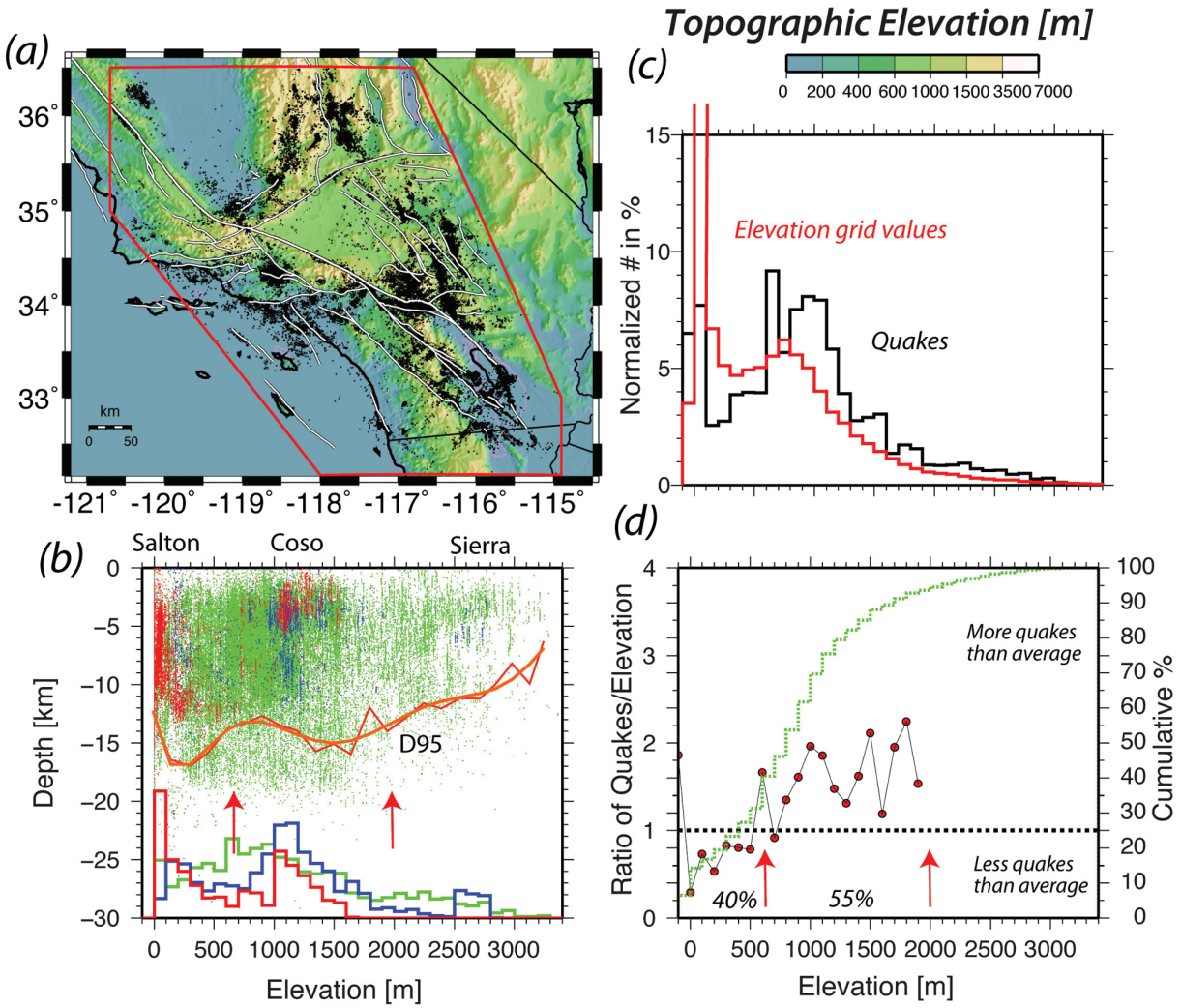

Figure 3. Topography and seismicity. (a) Earthquakes of $M \geq 1.8$ are plotted on top of the topography of southern California within the study area outlined by the red polygon. (b) Each hypocentre is plotted at the respective focal depth and corresponding elevation interpolated from the topographic map. Detailed and smooth versions of the 95 per cent maximum seismicity depth contour are plotted in orange colour. (Bottom) histograms separating the three ranges of heat flow values, 0–55 (blue), 55–110 (green) and 110–3000 (red) mW m^{-2}, with y = log10(1.0 + frequency percent) with full scale of 5.0. (c) Normalized histograms of quakes and 'elevation values' for each 100 m interval of elevation. (d) Ratio of the two histograms in (c) per 100 m interval in elevation (curve with red dots), and cumulative number of quakes (green curve). The arrows indicate the range of elevation where the percent (value shown in plot) of the seismicity occurs.

3.1.3 Isostatic gravity

The isostatic residual gravity anomalies represent a surface view of the 3-D distribution of spatial density variations at seismogenic depths within the middle to upper crust. The isostatic gravity data that we analyse are from Langenheim & Hauksson (2001) who compared the gravity data and the 3-D crustal *P*-wave velocity model of southern California. The positive gravity values represent the high-density mountain ranges, while the negative values represent the large basins. Large density contrasts are located where basins and mountains abut in the upper crust, or in rare cases they may reflect variations in the thickness of the lower crust (Fig. 4a).

The seismicity is distributed across the isostatic gravity field. The plot of focal depths of earthquakes versus the isostatic gravity at each epicentre shows that most of the earthquakes occurs within a limited negative range of isostatic gravity (Fig. 4b). The low (Sierra) and high heat flow (Coso and Salton Trough) regions are also located in this range. The D95 contour that shows a progressive increase in depth (from 13 to 17 km) for isostatic gravity from 0 to –45 mGal is not well constrained for higher and much lower (negative) isostatic gravity values.

The normalized histograms of evenly sampled isostatic gravity values and gravity values at epicentres exhibit almost identical patterns, with 85 per cent of the seismicity occurring at isostatic gravity values of –12 to –50.0 mGal (Figs 4c and d). An above average number of earthquakes occur in the range from –12 to 24 mGal, which includes major aftershock sequences such as the 1992 Landers sequence. At very low isostatic gravity values of <–40.0 mGal, below the major basins, there are small clusters of hypocentres scattered at average to shallow depth but they are always located at depths below the basin sediments. There is also a small population of earthquakes with isostatic gravity of >0.0 mGal, located along the eastern edge of the positive Peninsular Ranges isostatic gravity anomaly. These patterns suggest that earthquakes occur preferentially in mid to low-density crust but they are rare in high density or very low-density crust.

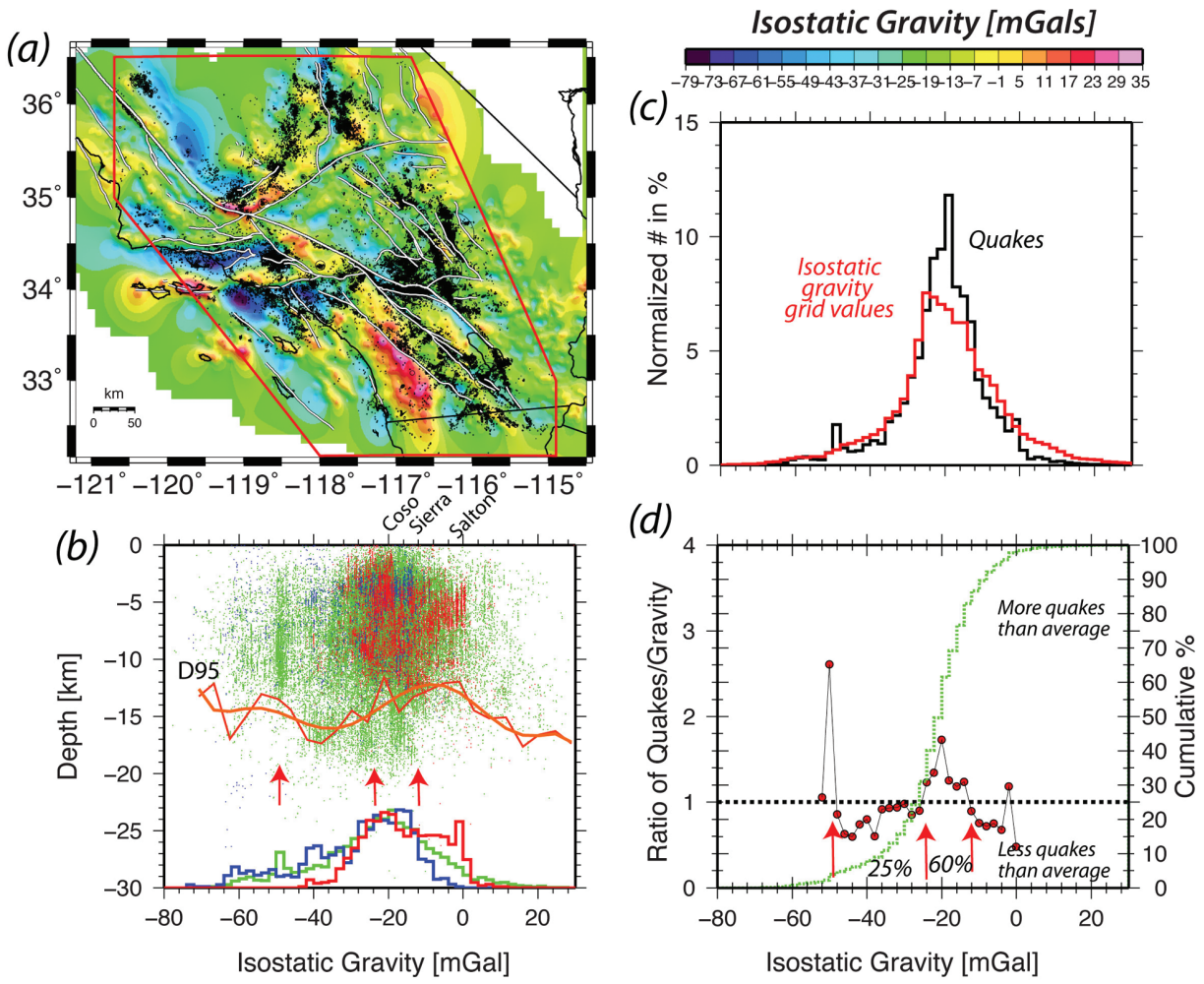

Figure 4. Isostatic Gravity and seismicity. (a) Earthquakes of $M \geq 1.8$ are plotted on top of the isostatic gravity map of southern California within the study area outlined by the red polygon. (b) Each hypocentre is plotted at the respective focal depth and corresponding isostatic gravity value interpolated from the map. Detailed and smooth versions of the 95 per cent maximum seismicity depth contour are plotted in orange colour. (Bottom) histograms separating the three ranges of heat flow values, 0–55 (blue), 55–110 (green) and 110–3000 (red) mW m^{-2}, with $y = \log10(1.0 + \text{frequency percent})$ with full scale of 5.0. (c) Normalized histograms of quakes and 'isostatic gravity values' for each 10 (mGal) interval of isostatic gravity. (d) Ratio of the two histograms in (c) per 10 (mGal) interval in isostatic gravity (curve with red dots), and cumulative number of quakes (green curve). The arrows indicate the range of isostatic gravity where the percent (value shown in plot) of the seismicity occurs.

3.1.4 Crustal average of V_p/V_s

The crustal V_p/V_s ratio can be viewed as a proxy for lithology, and in some cases for fluid content of the crust (Nakajima *et al.* 2001). We use V_p/V_s values from Yan & Clayton (2007) who used teleseismic receiver functions to determine V_p/V_s and crustal thickness for southern California. They assumed a constant V_p of 6.3 km s^{-1} and obtained average crustal values with similar contributions from the upper and lower crust. Their average V_p/V_s values for southern California of 1.73–1.78 agree with previous receiver-function results of Zhu & Kanamori (2000) and are consistent with the results of Hauksson (2000) who showed that V_p/V_s from a 3-D tomographic inversion mostly ranged from 1.7 to 1.8, with somewhat higher values in the sedimentary basins. These Yan & Clayton (2007) V_p/V_s estimates and the spatial density of earthquakes exhibit an irregular distribution across southern California (Fig. 5a). The low average V_p/V_s values are limited to areas such as the Santa Monica Mountains, south end of the Elsinore fault, the northwest Mojave Desert and parts of eastern California. In contrast, the southeastern Mojave Desert, parts of the Peninsular Ranges, Los Angeles and Ventura basin are characterized by high average V_p/V_s.

The plot of focal depths versus average V_p/V_s values at each of the epicentres shows that the seismicity occurred in crust with average V_p/V_s ranging from 1.68 to 1.84, with a small deep cluster of seismicity at $V_p/V_s \sim 1.76$ (Fig. 5b). Both Coso and Salton Trough seismicity occur at the high end of this range, while the Sierra seismicity occurs at the low end of the range. The maximum 95 per cent depth contour (D95) exhibits a small change in earthquake depths from 13 km depth at $V_p/V_s = 1.66$–16 km at $V_p/V_s = 1.84$.

The normalized histograms of evenly sampled V_p/V_s values and V_p/V_s values at epicentres exhibit a similar distribution, with most of the values in the range from 1.68 to 1.84 (Fig. 5c). Approximately 90 per cent of the seismicity occurred at depths from 2 to 12 km at locations where the crustal average V_p/V_s ranges from 1.74 to 1.84 (Fig. 5d). Because the average California crustal V_p/V_s is 1.72 (Brocher 2005), most of the southern California seismicity is occurring where vertically averaged V_p/V_s values are higher than

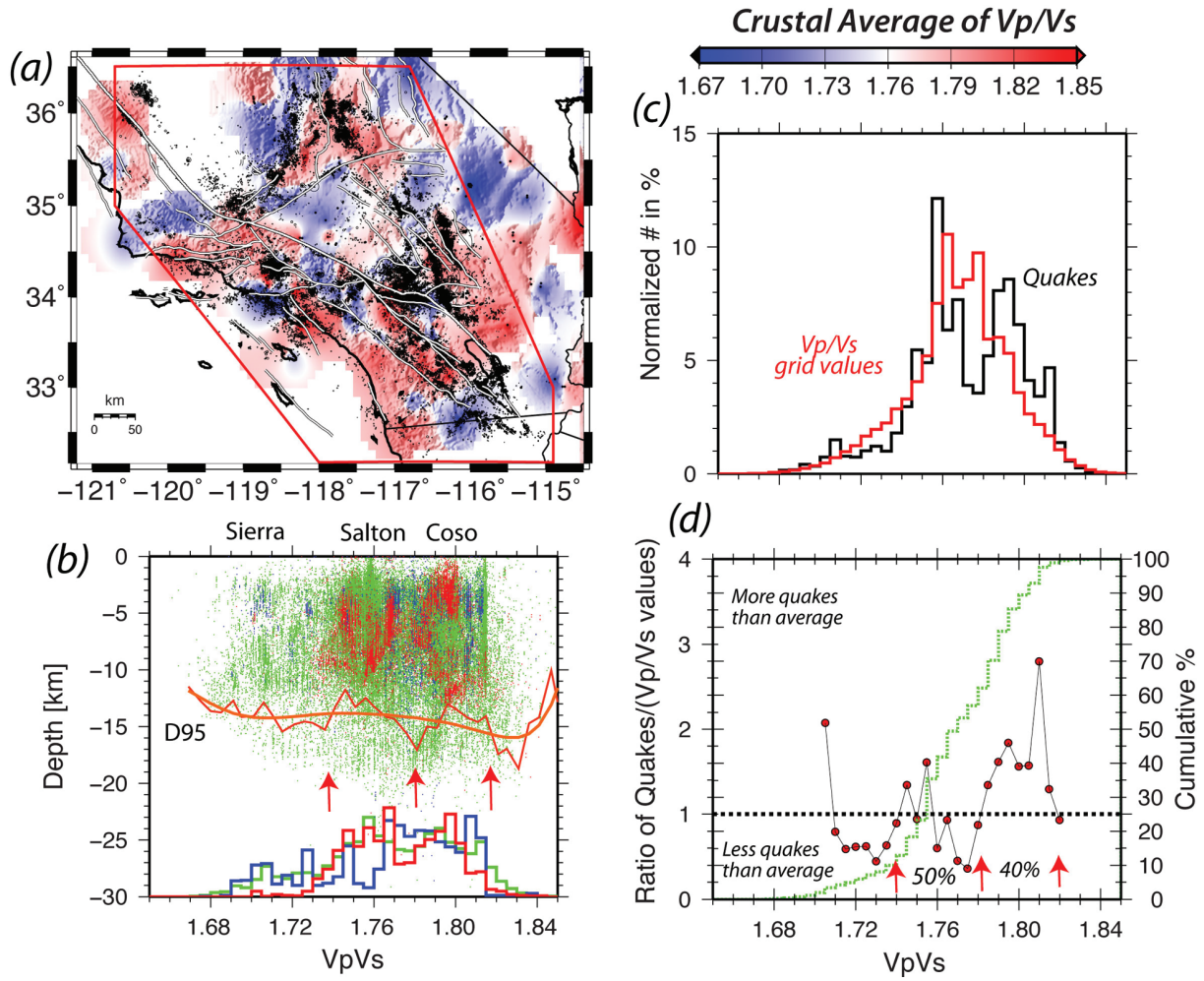

Figure 5. Crustal average of V_p/V_s and seismicity. (a) Earthquakes of $M \geq 1.8$ are plotted on top of the V_p/V_s crustal average map for southern California within the study area outlined by the red polygon. (b) Each hypocentre is plotted at the respective focal depth and corresponding V_p/V_s value interpolated from the map. Detailed and smooth versions of the 95 per cent maximum seismicity depth contour are plotted in orange colour. (Bottom) histograms separating the three ranges of heat flow values, 0–55 (blue), 55–110 (green) and 110–3000 (red) mW m^{-2}, with $y = \log10(1.0 +$ frequency percent) with full scale of 5.0. (c) Normalized histograms of quakes and 'V_p/V_s values' for each 0.01 interval of V_p/V_s. (d) Ratio of the two histograms in (c) per 0.01 step in V_p/V_s (curve with red dots), and cumulative number of quakes (green curve). The arrows indicate the range of V_p/V_s where the percent (value shown in plot) of the seismicity occurs.

the average, with an above average number of events at values from 1.78 to 1.82 (Fig. 5d).

In contrast, Lin & Shearer (2009) found that locally southern California seismicity has greater affinity for volumes with low V_p/V_s of 1.72 from tomography and V_p/V_s of 1.67 from similar event clusters. This difference is likely related to the receiver-function V_p/V_s values representing vertically averaged values for the whole crust while the tomographic and especially the *in situ* cluster based V_p/V_s values are local high-resolution measurements. In particular, the receiver function analyses compute V_p/V_s values using near-vertically travelling rays that average across crustal volumes with and without seismicity. Because the presence of fluid-filled cracks may affect the absolute values of V_p, V_s and V_p/V_s depending on the ray path and model averaging, the results of these measurements may simply reflect the different assumptions being applied by Lin & Shearer (2009).

Because rock composition can affect V_p/V_s, in particular lower V_p/V_s values are associated with quartz-rich rocks. The presence of fluids in the crust raises the V_p/V_s ratio, but depending upon the geometry of the cracks in some rare cases the V_p/V_s can be lowered (e.g. Nakajima *et al*. 2001; Takei 2002). Because the seismicity seems to prefer to occur within crust with above average V_p/V_s ratios or as suggested by Lin and Shearer (2009) in crustal volumes with fluid filled cracks of certain aspect ratios, we infer that fluids play a role in their occurrence.

3.1.5 *Crustal thickness*

We analyse the crustal thickness beneath southern California that varies from ∼22 to ∼43 km depth as determined by Yan & Clayton (2007). They used teleseismic receiver functions to determine regional variations in Moho depth (Fig. 6a). We added a few measurements to the depth of Moho in the Ventura basin area from Bryant & Jones (1992), and in the Salton Trough area from Magistrale *et al*. (2000). The shallowest Moho is found beneath the Continental Borderland and the Salton Trough. A deep Moho is found beneath a corridor that extends from the San Bernardino Mountains to the south across the Peninsular Ranges as well as the deepest part of the Ventura Basin. The deepest Moho exists beneath the high Sierra Nevada. Seismicity is scattered across all Moho depths (Fig. 6a).

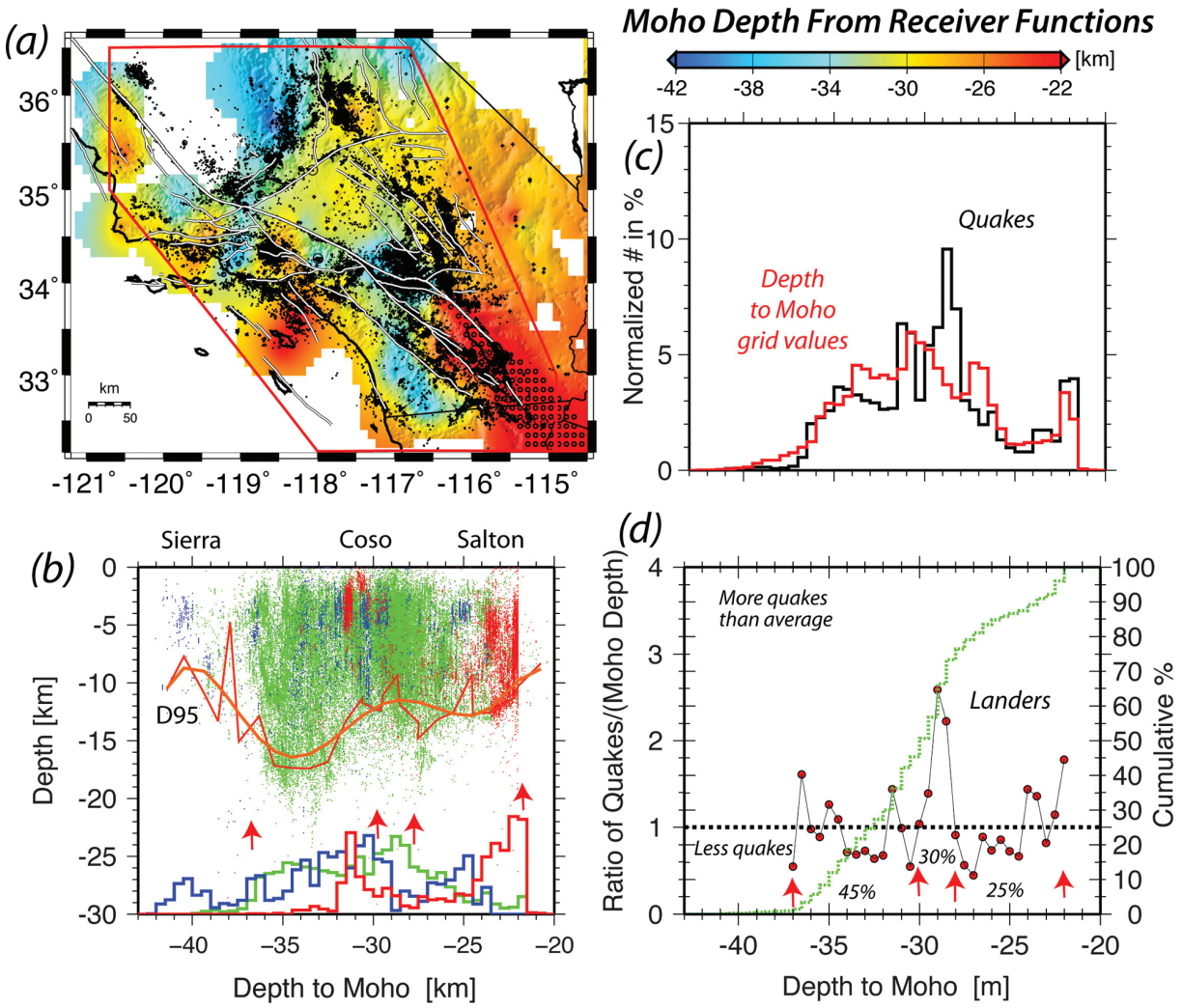

Figure 6. Moho-depth and seismicity. (a) Earthquakes of $M \geq 1.8$ are plotted on top of the Moho-depth map for southern California within the study area outlined by the red polygon. (b) Each hypocentre is plotted at the respective focal depth and Moho-depth interpolated from the map. Detailed and smooth versions of the 95 per cent maximum seismicity depth contour are plotted in orange colour. (Bottom) histograms separating the three ranges of heat flow values, 0–55 (blue), 55–110 (green) and 110–3000 (red) mW m^{-2}, with $y = \log10(1.0 + \text{frequency percent})$ with full scale of 5.0. (c) Normalized histograms of quakes and 'Moho-depth values' for each 100 m step of Moho-depth. (d) Ratio of the two histograms in (c) per unit Moho-depth (curve with red dots), and cumulative number of quakes (green curve). The arrows indicate the range of Moho-depth where the percent (value shown in plot) of the seismicity occurs.

The plot of the Moho-depth values at each epicentre and the corresponding focal depths show that seismicity preferentially occurs in the Moho-depth range of 22–37 km. There are also some scattered shallow earthquakes in the Moho-depth range of 37–43 km, which are located beneath the southern Sierra Nevada (Fig. 6b). The Salton Trough seismicity and the Coso seismicity are clearly separated by the different crustal thicknesses. The 95 per cent depths of earthquakes varies from ∼13 to ∼17 km as the Moho-depth changes from 22 to 35 km. For deeper Moho from 35 to 43 km the focal depths become quickly shallower, with 95 per cent depths shallowing to ∼10 km. If the crust is very thick, the seismicity appears to be mostly confined to the shallow part of the upper crust, like beneath the high Sierra Nevada. However, there are relatively few earthquakes in areas with crustal thickness that exceeds 37 km.

The normalized histograms of evenly sampled Moho-depth values, and Moho-depth values at epicentres exhibit similar distributions except for more than average earthquakes at the location of the Landers earthquake sequence (Fig. 6c). The above average peak of seismicity for the Moho-depth of 28–29 km is formed by the 1992 Landers aftershocks sequence. The far-right peak at 22 km Moho-depth is associated in part with seismicity related to geothermal activity, near the south end of the Salton Sea.

The ratio of number of Moho-depth values at epicentres and the corresponding number of Moho-depth values shows several smaller peaks where quake density is above average (Fig. 6d). The largest peak with 30 per cent of the seismicity occurs for Moho depths of 28–30 km, and corresponds to the Landers sequence. The overall absence of large clusters of above average or below average seismicity shows that seismicity is equally likely to occur in crustal thicknesses extending from 22 to 37 km.

3.1.6 Fault-distance

The Pacific–North America plate boundary in southern California consists of numerous late Quaternary faults that accommodate plate motion and account for geometrical irregularities in the plate boundary. The principal slip zones (PSZs) of the major late Quaternary faults are prominent geological features that have been compiled

into the Southern California Earthquake Center Community Fault Model (SCEC/CFM; Plesch *et al*. 2007). In particular, the PSZs accommodate major ($M > 7$) earthquakes that account for significant fraction of the North America Pacific Plate motions.

We use the SCEC/CFM and high precision earthquake locations (Lin *et al*. 2007) to precisely measure the distances between the individual hypocentres and the nearest PSZ (Hauksson 2010). We analyse these measured distances in the range from 0 to 20 km in southern California. The colour-coding with distance in Fig. 7(a) outlines most of the PSZs of the late Quaternary faults with the red coloured epicentres. These distance measurements are not static properties of the crust, but presuming that these are fairly representative seismicity patterns for any 25 yr time period, their average spatial distribution should be almost unchanged with time.

The plot of focal depths of earthquakes versus fault-distance for each epicentre show that earthquakes are most common closest to the PSZs, with a rapid decrease in the number of events away from the PSZs (Fig. 7b). The smoothed 95 per cent maximum depth suggests the presence of shallower 95 per cent maximum depth by ∼2 km next to the PSZs, although the un-smoothed 95 per cent maximum depth shows several local oscillations. Further away, the 95 per cent maximum depth increases from ∼14 km to ∼15 km depth, suggesting almost no influence on depth, for earthquakes located farther away than 2 km from the PSZs. Seismicity in the Salton Trough and Coso areas are separated in Fig. 7(b), both by depth and small fault distances.

The normalized histograms of epicentres to fault distances is peaked closest to the fault and reaches background at 5 km distance (Fig. 7c). In contrast, the distances measured from a regular grid of points across southern California show no clustering next to the PSZs. Thus earthquake density is highest closest to the PSZs, with 80 per cent of seismicity within 5 km distance of the PSZs, which includes both background seismicity and aftershocks, and decays rapidly with distance (Fig. 7d). Because faults are zones of crustal weakness, the density and spatial patterns of seismicity are to some extent influenced by crustal strength as represented by the geographical location and geometrical configuration of the late Quaternary faults. These results are similar to the results of Hauksson (2010) who separated out faults dominated by aftershocks, and faults dominated by interseismic seismicity. For instance, removing the aftershocks from the data set would simply provide fewer events in the distance range of 0–2 km but the overall decay of seismicity with distance from the PSZs would be similar.

3.2 Kinematic crustal parameters

The three kinematic crustal parameters are derived from GPS measurements and upper mantle flow modelling. They provide a view of how the plate tectonic strain rate field deforms the California crust.

3.2.1 Shear strain rate

The relative Pacific–North America plate motion results in a shear strain rate field that has a significant effect on the 3-D spatial distribution of seismicity. To first order the shear strain rate field is constant with depth. We analyse the shear strain rate from Tape *et al.* (2009) who used wavelets to fit GPS data collected in southern California and determine the shear strain rate. Their GPS derived surface shear strain rate and the spatial density of earthquakes vary across southern California (Fig. 8a). The highest strain rates of $>2.5 \times 10^{-7}$ strain yr^{-1} are centred near Parkfield and the Salton Trough where the plate motion is accommodated in a narrow, possibly creeping, region. Other regions that exhibit significant seismicity are characterized by average strain rate of 1.0 to 2.0×10^{-7} strain yr^{-1}. Several regions of low strain rate, such as the northeast Mojave, southern Sierra Nevada and the offshore area from Malibu to Point Mugu exhibit moderate background seismicity. This could be due to the lack of resolution in the strain rate field. Alternatively, other crustal deformation processes could cause this seismicity rather than shear strain rate build-up along the plate boundary.

The plot of focal depths and corresponding shear strain rate values at each of the epicentres show that most of the earthquakes occur at low to moderate strain rates (Fig. 8b). The 95 per cent maximum depth distribution increases from 12 to 15 km at strains of 2.0×10^{-7} strain yr^{-1}. At higher strain rates, where 15 per cent of the seismicity occurs, the 95 per cent depth becomes shallower, and ends at ∼10 km depth. This seismicity occurred mostly near Parkfield and in the Salton Trough. The Coso seismicity occurs with the range of average strain rate suggesting that Coso region is not experiencing an anomalous strain rate.

The normalized histogram of evenly sampled strain rate values and heat flow values at epicentres show to separate peaks, showing the preference of the seismicity to occur at average strain rate values (Fig. 8c). The ratio of the two histograms shows that there is more than average seismicity or 60 per cent of the total rate in the shear strain rate range of 1.1 to 2.6×10^{-7} (Fig. 8d). Because the thickness of the seismogenic zone affects the spatial distribution of the strain rate field, the high shear strain rate field is concentrated in a narrow zone along the plate boundary, and the moderate strain rate field is distributed further away, where most of the seismicity is concentrated.

3.2.2 GPS derived surface strain rate dilatation

The dilatation crustal deformation field that causes crustal thinning or thickening is superimposed on the shear deformation as part of the plate boundary deformation processes. Fay *et al.* (2008) combined GPS based velocity solutions to estimate the dilatation rate or the rate of changes in crustal thinning or thickening across southern California. We compare their GPS measured surface strain rate dilatation with the spatial density of earthquakes (Fig. 9a). To first order the dilatational crustal strain rate field is constant with depth. Negative strain rate dilatation or crustal thickening occurs in the western Transverse Ranges and the western Great Valley as well as the California Coast Ranges and along the While Wolf fault system (Argus & Gordon 2001). Crustal thinning occurs in eastern California, including the Eastern California Shear Zone and the Salton Trough region.

The data in the plot of focal depths and corresponding strain rate dilatation values at each of the epicentres show that most of the earthquakes occur within regions of crustal thinning (Fig. 9b). The maximum 95 per cent depth is highly variable but shows average shallowing from ∼16 to ∼12 km from compressional to extensional strains of –50 to 50 nanostrains yr^{-1}. However, beyond this range, in the range of <–50 nanostrains yr^{-1} (large compressional dilatation), there is also a prominent increase in the depth of earthquakes. These earthquakes, in regions of very negative strain rate dilatation values, occur below the Central Valley, the southern Mojave and the western Transverse Ranges Ventura and Los Angles basins. The Coso seismicity and the Salton Trough seismicity both occur at slightly negative and slightly positive crustal dilatation.

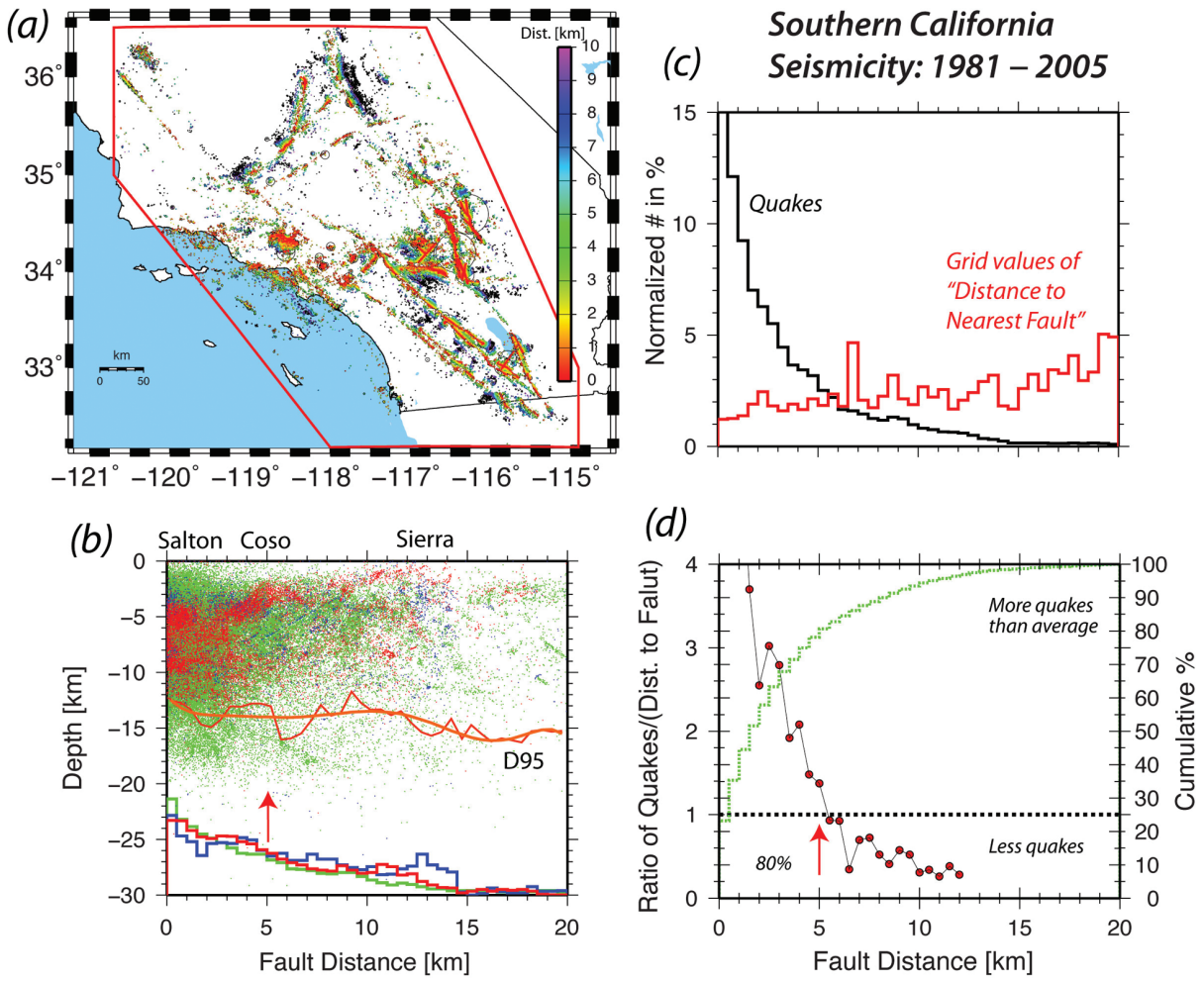

Figure 7. Fault-distance and seismicity. (a) Fault-distances for earthquakes of $M \geq 1.8$ are plotted in colour; the study area outlined by the red polygon. The late Quaternary mapped fault traces are not included. (b) Each hypocentre is plotted at the respective distance from the nearest principal slip-surface of a late Quaternary fault. Detailed and smooth versions of the 95 per cent maximum seismicity depth contour are plotted in orange colour. (Bottom) histograms separating the three ranges of heat flow values, 0–55 (blue), 55–110 (green) and 110–3000 (red) mW m^{-2}, with $y = \log10(1.0 + \text{frequency percent})$ with full scale of 5.0. (c) Normalized histograms of quakes and 'fault-distance' values for each 1 km of distance, and relative density of distances measured from a regular grid across southern California. (d) Ratio of the two histograms in (c) per 1 km step in fault-distance (curve with red dots), and cumulative number of quakes (green curve). The arrows indicate the range of fault-distances where the percent (value shown in plot) of the seismicity occurs.

The normalized histograms of strain rate dilatation values and strain rate dilatational values at epicentres are similar across southern California, though seismicity is more common at positive strain rate values (Fig. 9c). The ratio of numbers of strain rate dilatation values at epicentres divided by the number of equally spaced dilatation values shows that more than average seismicity occurs between strain rate values of 15 and 55 nanostrain yr^{-1} (Fig. 9d). A small cluster of above average density of seismicity is also observed at negative strain rate values of –65 to –80 nanostrain yr^{-1}. This pattern shows that seismicity occurs preferentially in areas of crustal thinning, and the compressional stresses need to reach a certain size to cause seismicity. Further, the deepening of seismicity with large negative dilatation suggests that the crustal thickening significantly affects D95 depth of seismicity.

3.2.3 Modelled crustal dilatation rate

Fay *et al.* (2008) also predicted crustal deformation across southern California using their geodynamic model with uniform upper-mantle viscosity. They determined the relative horizontal dilatation rate using the strain rate tensor at 20 km depth. Using the model they identified regions of negative dilatation of crustal thickening in areas of down welling mantle. Similarly, they identified regions of upwelling and divergent flow of the upper mantle that caused positive dilatation or crustal thinning.

The model-derived relative crustal dilatation and the spatial density of earthquakes vary across southern California (Fig. 10a). The seismicity is about evenly distributed between positive and negative dilatations. The data in the plot of focal depths and of the modelled crustal dilatation at each of the epicentres show that the earthquake depths increase from positive to negative dilatation (Fig. 10b). The 95 per cent maximum depth ranges from ∼8 to ∼16 km. The Coso seismicity and the Salton Trough seismicity both occur at the high relative crustal dilatation.

This strong increase in depth is similar to the increase in seismicity depth observed for increasing crustal thickness (Fig. 6b). This similarity, suggest that the modelled crustal dilatation by Fay

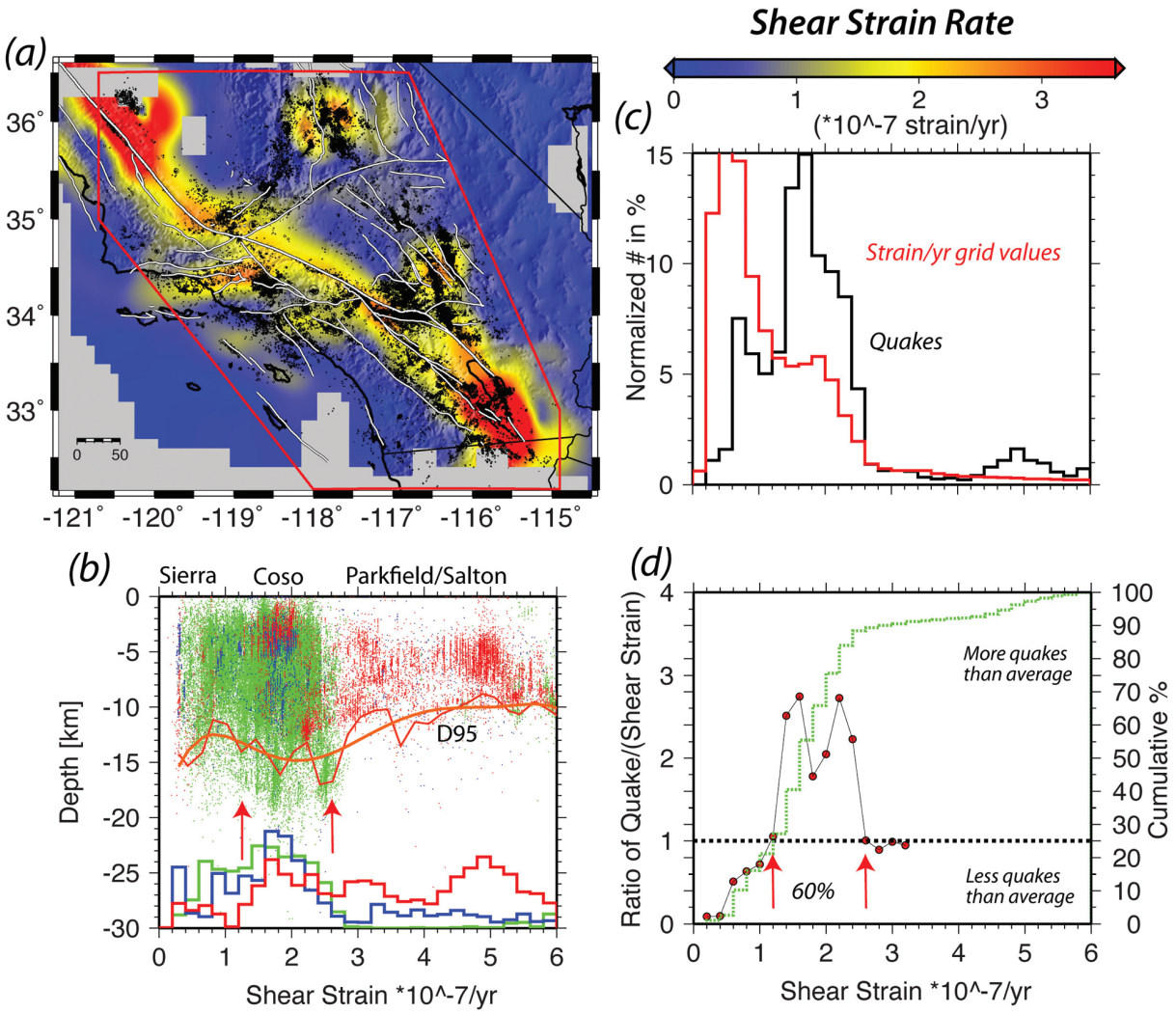

Figure 8. Shear strain rate derived from GPS, and seismicity. (a) Earthquakes of $M \geq 1.8$ are plotted on top of the shear strain rate map of southern California within the study area outlined by the red polygon. Detailed and smooth versions of the 95 per cent maximum seismicity depth contour are plotted in orange colour. (b) Each hypocentre is plotted at the respective focal depth and corresponding shear strain rate from the map. (Bottom) histograms separating the three ranges of heat flow values, 0–55 (blue), 55–110 (green) and 110–3000 (red) mW m^{-2}, with $y = \log10(1.0 +$ frequency percent) with full scale of 5.0. (c) Normalized histograms of quakes and 'strain rate values' for each 0.02 units of strain rate. (d) Ratio of the two histograms in (c) per 0.05 step in strain-rate (curve with red dots), and cumulative number of quakes (green curve). The arrows indicate the range of strain-rate where the percent (value shown in plot) of the seismicity occurs.

et al. (2008) is strongly dependent on crustal thickness. Possibly, the variations in crustal thickness cause large density contrast in the model across the Moho, and may exert a strong influence on the calculated modelled dilatation.

The normalized histograms of evenly spaced model dilatation values and dilatation values at each of the epicentres exhibit a similar distribution from –0.4 to 0.6 relative strain. At negative dilatation, at relative strain rates of about –0.4 and less, the number of earthquakes decreases significantly.

The ratio of the number of dilatation values at epicentres and modelled dilatation values shows two ranges with more than average earthquakes (Fig. 10d). The first has relative dilatational values from 0.2 to 0.6 while the second has dilatational values from –0.1 to –0.4. The shallowest distribution of earthquakes occurs at the most positive strain rates. This pattern suggests that crustal thickness has a strong influence on the mantle flow in the Fay *et al.* (2008) model.

3.3 Crustal temperature

To determine the crustal temperature, we apply the 1-D heat flow equation to calculate the temperature as a function of depth within the crust (Bonner *et al.* 2003). The Fourier law for 1-D vertical steady-state heat flow can be expressed as

$$k\mathrm{d}^2T/\mathrm{d}z^2 = -A(z), \tag{1}$$

where k is the thermal conductivity, T is the temperature, z is depth and A is the heat production (Tanaka & Ishikawa 2002).

Radioactive heat generation that contributes to the temperature of the continental crust decays exponentially with depth (Lachenbruch 1970). For the heat flow, Tanaka & Ishikawa (2002) showed that the temperature (T) as a function of depth (z) is given by

$$T = T_0 + ((q_0 - Az_1)/k)z + \left(Az_1^2/k\right)(1 - \exp(-z/z_1)), \tag{2}$$

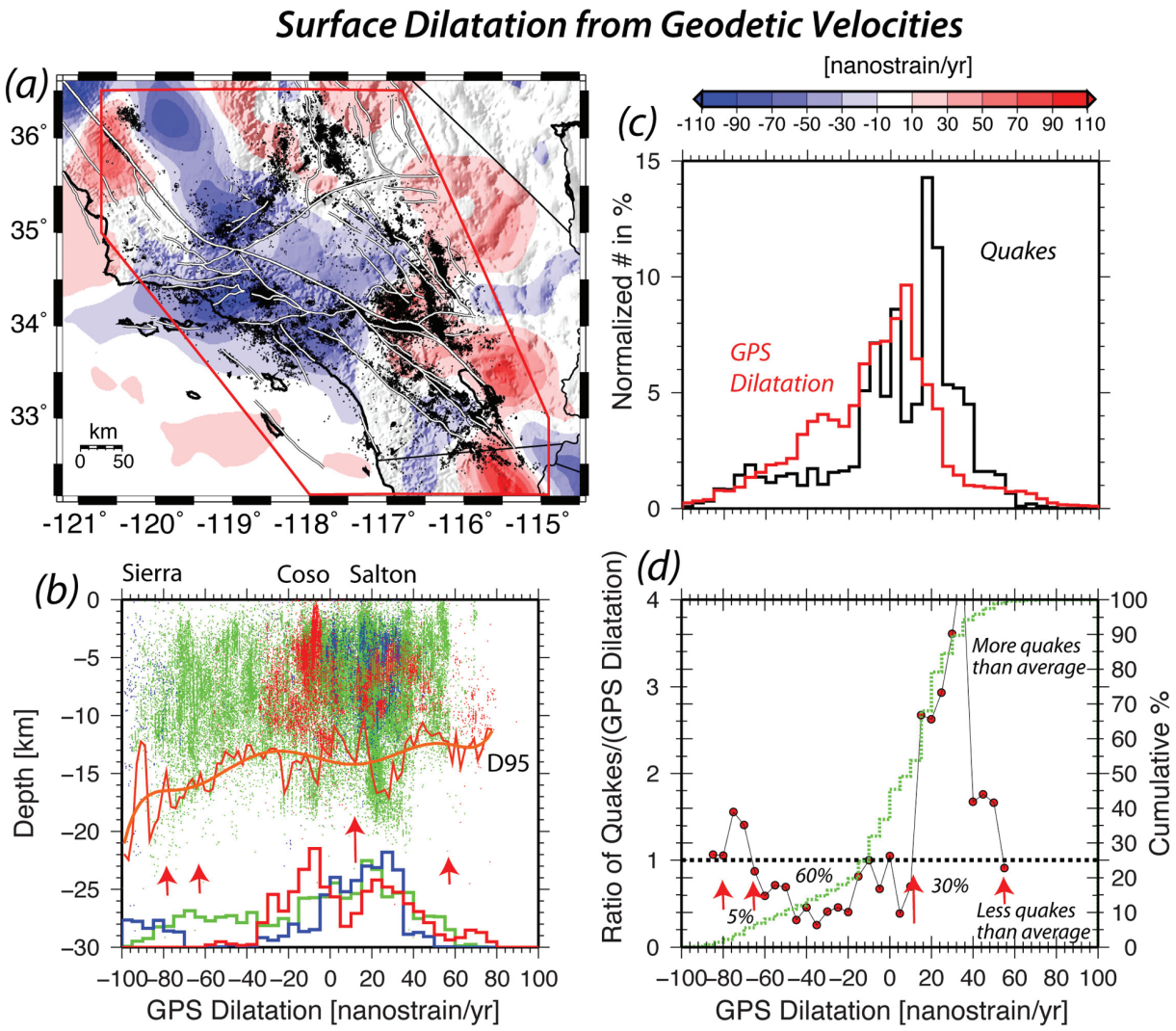

Figure 9. GPS measured surface strain rate dilatation and seismicity. (a) Earthquakes of $M \geq 1.8$ are plotted on top of the surface strain rate dilatation of southern California within the study area outlined by the red polygon. (b) Each hypocentre is plotted at the respective focal depth and corresponding surface strain rate dilatation interpolated from the map. Detailed and smooth versions of the 95 per cent maximum seismicity depth contour are plotted in orange colour. (Bottom) histograms separating the three ranges of heat flow values, 0–55 (blue), 55–110 (green) and 110–3000 (red) mW m^{-2}, with $y = \log10(1.0 +$ frequency percent) with full scale of 5.0. (c) Normalized histograms of quakes and 'dilatation strain values' for each 5 units of dilatation strain. (d) Ratio of the two histograms in (c) per 5 units step in dilatation strain (curve with red dots), and cumulative number of quakes (green curve). The arrows indicate the range of strain-dilatation where the percent (value shown in plot) of the seismicity occurs.

where q_0 is heat flow, the thermal conductivity within the California crust (k) is 2.5 Wm^{-1}K^{-1} and the average heat generation (A) is 1.7 μ Wm^{-3} (Bonner *et al.* 2003). The constant values are from Tanaka & Ishikawa (2002); $z_1 = 10$ km, $T_0 = 13.4$ °C. In a previous study, Bonner *et al.* (2003) applied the equation above to determine the temperature isotherms for the California crust.

Using our data set of heat flow versus Moho-depth we derive the following empirical relationship between heat flow and Moho-depth (D) in km

$$q_0 = B - C * D, \tag{3}$$

where B is the average heat flow at the surface and C is the empirically determined heat flow depth gradient (Fig. 11). A linear fit provides $B = 110.2$ (mW m^{-2}) and $C = 1.4$ (mW m^{-2} km^{-1}). We insert eq. (3) into eq. (2) and determine the temperature isotherms in the 2-D space of focal-depth and Moho-depth (Fig. 12). These temperature isotherms deepen with increasing crustal thickness. The clear increase in depth of seismicity with thicker crust from 22 to 37 km is bracketed at depth by the ∼400 °C isotherm. The coherent relationship between the focal depths and the Moho depths suggest that parameters other than temperature, such as lithology, play a minor role in influencing earthquake depths.

The deepening of the isotherms and the abrupt shallowing in focal depths at 37 km could be caused by the increased crustal thickness and corresponding increase in normal force being too high to allow rupture of the whole depth range of the brittle-ductile transition zone. Thus the earthquakes in the shallow part of very thick crust may signify other processes than plate tectonic boundary motion.

The apparent streaks of deep events, below ∼400 °C, could be the effects of larger sequences that temporarily extend into the ductile lower crust. This observation is consistent with transient deepening of seismicity following large events, which is generated in the regional lithospheric model of Ben-Zion and Lyakhovsky (2006) with a crust governed by damage rheology over a viscoelastic substrate.

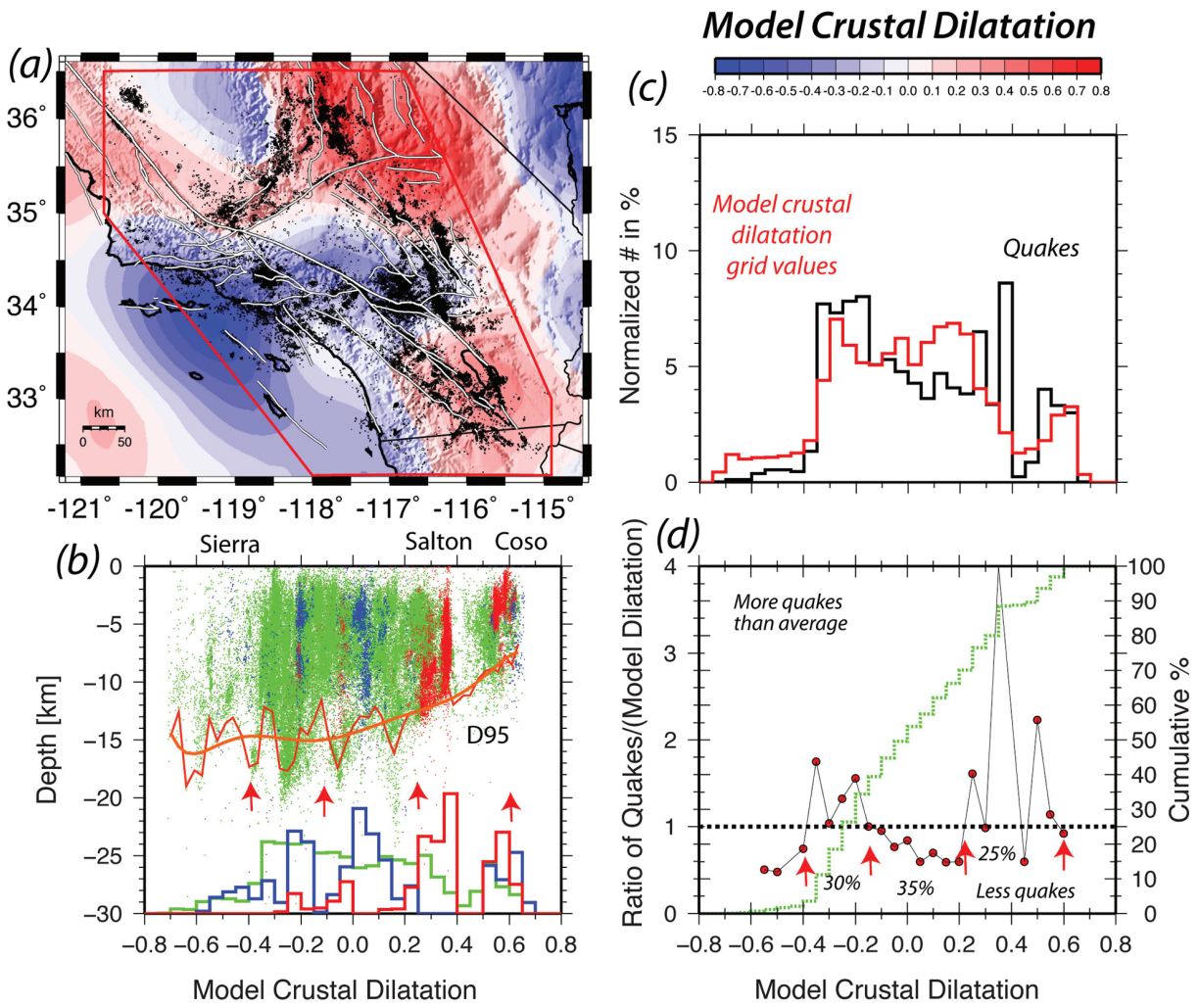

Figure 10. Modelled crustal dilatation and seismicity. (a) Earthquakes of $M \geq 1.8$ are plotted on top of the modelled dilatation of southern California within the study area outlined by the red polygon. (b) Each hypocentre is plotted at the respective focal depth and corresponding modelled dilatation from the map. Detailed and smooth versions of the 95 per cent maximum seismicity depth contour are plotted in orange colour. (Bottom) histograms separating the three ranges of heat flow values, 0–55 (blue), 55–110 (green) and 110–3000 (red) mW m^{-2}, with $y = \log10(1.0 + \text{frequency percent})$ with full scale of 5.0. (c) Normalized histograms of quakes and 'modelled dilatation values' for each 0.05 units of modelled dilatation. (d) Ratio of the two histograms in (c) per 0.05 interval in modelled (curve with red dots), and cumulative number of quakes (green curve). The arrows indicate the range of model crustal dilatation where the percent (value shown in plot) of the seismicity occurs.

Alternatively, they could be caused by special geological conditions such as crustal delamination processes beneath the Ventura Basin and Banning Pass (Magistrale 2002). It is unlikely that they could also be artefacts of the interpolation of the Moho-depth data or poorly determined focal depths.

The line with slope of 1.0 in Fig. 12 represents the Moho boundary that separates the crust and mantle. This line demonstrates that the thickness of the lower crust changes twice as fast as the thickness of the upper crust. A few earthquakes that apparently seem to locate within the mantle may have poorly determined focal depths.

4 DISCUSSION

The joint analysis of the seismicity and the geophysical parameters that describe the properties of the southern California crust provides insight into which parameters appear to exert the strongest influence on the spatial distribution of seismicity. Our analysis shows that the most important parameters are the fault-distance and the crustal thickness while heat flow as well as other parameters are less influential.

In this study, we have focused on analysing the geophysical parameters and seismicity on a broad regional scale. However, it is possible that if southern California were divided into tectonic regions such as the strike-slip faulting San Andreas fault system, thrust faulting Transverse Ranges, and extensional faulting in the Salton Trough, additional regional details in the relationship between the geophysical parameters and seismicity could be resolved.

4.1 Crustal geophysics parameters and seismicity

The spatial variations in both static and kinematic crustal geophysical parameters influence locally both the geographical and depth distribution of the seismicity. In Table 1 we provide the mean, median and standard deviation values that characterize the values of the geophysical parameters. We also provide the range of each parameter referred to the median value.

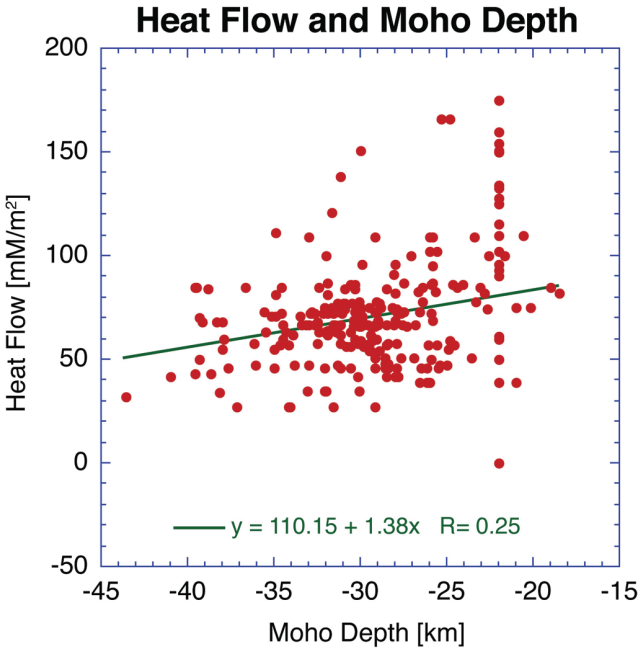

Figure 11. Regression of heat flow and depth to Moho using data from Yan and Clayton (2007).

Approximately, 68 per cent of the earthquakes occur within a certain range of each of the modelled geophysical variables. When referenced to the median value the seismicity occurs within the heat flow range from 55 to 98 mW m^{-2}, topography 0.3–1.4 km, isostatic gravity from –28 to –11 mGal, fault distance of 0.0–3.6 km, crustal average V_p/V_s 1.74–1.80, and depth to Moho from 26 to 33 km. Further, the seismicity occurs at shear strain rate values of 1.06–2.38 strain × 10^{-7} yr^{-1}, and GPS measured dilatation from –12 to 36 nanostrains yr^{-1} as well as modelled relative dilatation of –0.36–0.37.

Initially, we expected that heat flow would play a dominant role in determining the spatial or the focal depth distribution but because most of the seismicity occurs in a limited range of heat flow values, ∼50–∼110 mW m^{-2}, the heat flow values are not particularly diagnostics of the spatial distribution of seismicity or the focal depth variations (Fig. 2). However, very low and very high heat flow values characterize the high Sierra Nevada, and known geothermal areas such as Coso and the Salton Trough. The Coso and Salton Trough geothermal areas differs in that Coso is in normal crust characterized by shallow seismicity, but the Salton Trough is characterized by thin crust and the seismicity extends through the whole brittle crust.

The other static parameters, besides heat flow, such as topography, isostatic gravity, average V_p/V_s and Moho depth, include some limited value ranges with above or below average seismicity. In most cases, the above average values occur because of aftershock sequences, such as 1992 Landers, 1994 Northridge and 1999 Hector Mine. The below average seismicity areas may be due to the 25 yr catalogue not being long enough to provide a complete measurement of the seismicity rate. In particular, isostatic gravity shows that high heat flow earthquakes occur in areas of most common isostatic gravity values.

Each of these parameters seems to influence the distribution of 95 per cent of maximum focal depths (D95) in different ways. The D95 curves show both short wavelength variations, and long-term trends. The short wavelength variations could be local seismicity sampling

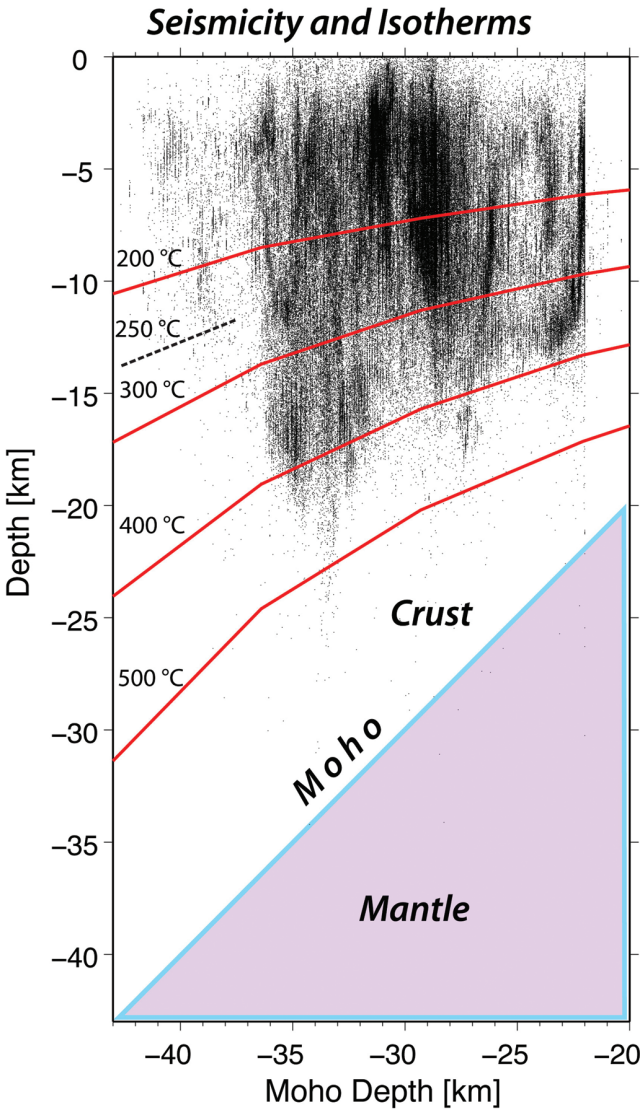

Figure 12. Focal depth versus Moho-depth, including temperature isotherms, and the Moho boundary. The line with slope 1.0 represents the Moho in this plot.

issues as well as due to the occurrence of individual earthquake sequences. The long wavelength variations may be real, indicating that certain ranges of parameter values allow seismicity to extend to greater depths. The heat flow range of 50–100 mW m^{-2} shows localized increase in D95 while the overall trend exhibits a decrease in focal depth with increasing heat flow. The effects of topography are similar, with D95 becoming more shallow beneath high elevation topography. The isostatic gravity and V_p/V_s show similar trends with shallow D95 for high density and high V_p/V_s. Similarly, the shear and volumetric strains also influence the seismicity depth with the deepest seismicity occurring at moderate strain rate values.

4.2 Late quaternary faults

The location of the late Quaternary faults that are zones of weakness exhibits the strongest influence on the geographical distribution of the recent (1981–2005) seismicity (Fig. 7). The late Quaternary faults such as the San Andreas, San Jacinto and Elsinore faults cut through large regions of southern California that are

Table 1. The statistical parameters [mean, standard deviation, median and mean absolute deviation (MAD)] for each of the geophysical parameters assigned to each earthquake.[a]

Geophysics Parameters	Mean Value	Standard Deviation	Median Value	MAD	68 per cent Range Referred to Median
Heat flow (mW m^{-2})	117.0	177.9	76.46	21.27	55.2–97.7
Topography (km)	0.885	0.638	0.861	0.555	0.31–1.42
Isostatic gravity (mGal)	−20.9	11.7	−19.9	8.35	−28.2 to –11.5
Fault-distance (km)	3.2	2.31	1.9	1.4	0.5–3.3
Average V_p/V_s	1.77	0.03	1.77	0.03	1.74–1.80
Moho-depth (km)	29.6	3.9	29.6	3.4	26.2–33.0
Shear strain (strain × 10^{-7} yr^{-1})	1.94	1.11	1.72	0.66	1.06–2.38
GPS dilatation (nanostrain yr^{-1})	2.82	31.3	11.62	24.0	−12.4–35.6
Model dilatation	0.045	0.296	0.0056	0.365	−0.36–0.37

[a]Also see the corresponding figures for more information.

characterized by average crust such as the central parts of the Mojave Desert, Transverse Ranges and Peninsular Ranges. The background seismicity forms spatial distributions that are centred on the PSZs of these faults, and thus is located within average crust (Hauksson 2010). About 85 per cent of the seismicity that includes both mainshock–aftershock sequences and background seismicity occurs within a distance of 5 km of the PSZs.

The average crust is characterized by regional heat flow ranges from 50 to 100 mW m^{-2}, and moderate values of other geophysical parameters such as topography, isostatic gravity and average V_p/V_s. The late Quaternary faults that accommodate plate motion in crust with average properties thus must have formed due to other influences such as special upper mantle conditions or particular geometry of plate boundary tectonic loading.

Similarly, the shear strain rates are average along the major late Quaternary faults. Although high shear strain rates exist near Parkfield and the Salton Trough, the seismicity does not concentrate in those areas (Fig. 8). The variations in volumetric strain rate are spread over broader areas and only exhibit large-scale variations (Fig. 9). The seismicity occurs preferentially in areas of crustal extension, although these areas do not coincide with the late Quaternary faults. Because the current strain rate fields are caused by both plate tectonic motion as well as mantle convection, they need not exhibit a simple relationship with the spatial distribution of the seismicity.

4.3 Crustal thickness

The crustal thickness that varies from 22 to 43 km beneath southern California has profound effects on the temperature distribution within the crust. The two extremes of thick (>37 km) and thin (<26 km) crust exhibit some special effects.

Thick crust is found in southern California beneath the Sierra Nevada (Yan & Clayton 2007). This crust is characterized by relatively low-density and high elevation, and the isotherms are deep. The relatively few earthquakes that are present within the Sierra Nevada are confined to shallow depths because the crust is too thick and too cold to accommodate faulting at greater depths, which is needed to accommodate tectonic plate motion. Unruh & Hauksson (2009) showed that gravitational collapse of the southern Sierra Nevada was the most likely mechanism that explained the shallow seismicity. In particular, the focal mechanisms showed extension in both the north–south and east–west directions. However, tectonic faulting that cuts through the seismogenic zone exists at the edges of the Sierra Nevada. The negative isostatic gravity and the low V_p and low V_p/V_s suggest quartz-rich crust where fluids are mostly absent (Hauksson 2000; Nakajima *et al*. 2001). Both the GPS-measured crustal dilatation and the model dilatation are positive, indicating ongoing crustal thinning processes.

The other two areas of thick crust have deep seismicity associated with them. The deep normal faulting seismicity beneath the Ventura basin is related to rapid crustal thickening (Bryant & Jones 1992). The region of relatively thick crust that extends across the Peninsular Ranges has some associated deep seismicity along its whole length, with clustered deep seismicity to the north in the Banning Pass region. The crust in these regions has geophysical properties that are between the properties of thick and average crust.

Thin crust usually implies a shallow brittle ductile transition zone as well as crustal thinning and ongoing crustal extension. Such crust is found beneath the Salton Trough and in the offshore continental borderland. The Salton Trough region is characterized by many closely spaced seismically active faults that accommodate both large mainshocks and frequent background seismicity swarms. Such swarms may be caused by transitory overpressures of fluids (Sibson & Rowland 2003). It is also a major sedimentary basin floored by a denser lower crust (Langenheim & Hauksson 2001). The crust is characterized by a high V_p/V_s ratio and negative dilatational strains, most likely because hot material is rising beneath it.

4.4 Crustal isotherms

The illumination of the southern California crust with seismicity reveals the regional effects, where the isotherms increase in depth with increasing crustal thickness (Fig. 12). The crustal earthquakes that occur in average crust at temperatures less than 400 °C are caused by frictional instability on existing fault surfaces. In this temperature range, quartz and feldspatic rocks become progressively more plastic with increasing temperature (Sibson 1984).

The heat flow in the continental borderland increases to the east, and most likely causes the strength of the crust to decrease as compared to the oceanic crust to the west, as well as the presence of ubiquitous volcanic rocks (Krause 1965). The continental borderland also has occasional earthquake swarms and accommodated the 1986 M_L 5.3 Oceanside sequence that exhibited an unusually high rate of aftershock activity (Hauksson & Jones 1988).

Our results are also consistent with global studies of the thickness of the lithosphere. These studies show that the thickness of the lithosphere has the most significant influence on continental geology because the thickness of the lithosphere reduces the temperature of the crust (Jackson *et al.* 2008). Similarly, in southern California the crustal thickness reduces the temperature of the crust and influences the distribution of seismicity.

5 CONCLUSIONS

Southern California (1981–2005) seismicity clusters near the late Quaternary faults, which accommodate the relative Pacific and North America plate movement in the crust with typically average geophysical properties. The proximity of seismicity, including mainshock–aftershock sequences and background seismicity, to late Quaternary faults has a much stronger influence on the distribution of seismicity than other geophysical crustal parameters, such as heat flow, isostatic gravity, shear strain rate and volumetric strain rates.

Variations in crustal thickness cause different scales of localization of deformation. Only sparse seismicity is present if the crust is thick, or dense with minimal quartz content, or the elevation high. This is consistent with crustal faults not extending through the thick crust of the major mountain ranges, and instead forming through going crustal faults at lower elevations. Similarly, if the crust is thin, the heat flow is very high, and topography is low, the seismogenic zone is also thin. The kinematic volumetric strains as well as modelling of the dilatational strain rate field favour earthquakes in extensional regimes, with some earthquakes in the compressional regime only if the strain rate is high enough.

The crustal isotherms increase in depth with increasing crustal thickness. The ∼400 °C isotherm forms the base of the seismogenic zone for crustal thickness from 22 to 37 km. At greater depths, 37–43 km, the ∼250 °C isotherm forms the base of the seismogenic zone. The deepening of the isotherms with increasing crustal thickness, and the systematic shallowing in focal depths at depths greater than 37 km is caused by the increased crustal thickness and possibly absence of fluids. Thus earthquakes in the shallow part of very thick crust may signify other processes than plate tectonic motion.

ACKNOWLEDGMENTS

This research was supported by the U.S. Geological Survey Grant G10AP00017 and G11AP20032 to Caltech, and by the Southern California Earthquake Center. SCEC is funded by NSF Cooperative Agreement EAR-0529922 and USGS Cooperative Agreement 07HQAG0008. Most figures were done using GMT (Wessel & Smith 1998). H. Kanamori suggested the formulation in Appendix. L. Jones, M. Simons and W. Yang provided helpful comments. N. Fay provided the data used for the GPS dilatation and the modelled dilatation. C. Tape provided the data for the shear strain field. A. Plesch provided distance measurements between each hypocentre to the nearest PSZ. SCEC contribution number 1446. Contribution number 10052, Seismological Laboratory, Division of Geological and Planetary Sciences, California Institute of Technology, Pasadena.

REFERENCES

Argus, D. F. & Gordon, R.G., 2001. Present tectonic motion across the Coast Ranges and San Andreas fault system in central California, *Geol. Soc. Am. Bull.,* **113**(12), 1580–1592, doi:10.1130/0016-7606(2001)113<1580:PTMATC>2.0.CO;2.

Ben-Zion, Y., 2008. Collective behavior of earthquakes and faults: continuum-discrete transitions, progressive evolutionary changes, and different dynamic regimes, *Rev. Geophys.,* **46,** RG4006, doi:10.1029/2008RG000260.

Ben-Zion, Y. & Lyakhovsky, V., 2006. Analysis of aftershocks in a Lithospheric model with seismogenic zone governed by damage rheology, *Geophys. J. Int.,* **165,** doi:10.1111/j.1365-246X.2006.02878.x

Bonner, J. L., Blackwell, D.D. & Herrin, E.T., 2003. Thermal constraints on earthquake depths in California, *Bull. seism. Soc. Am*., **93**(6), 2333–2354.

Brocher, T. M., 2005. Empirical relations between elastic wavespeeds and density in the Earth's crust, *Bull. seism. Soc. Am.* **95,** 2081–2092.

Bryant, S.A. & Jones, L.M., 1992. Anomalously deep crustal earthquakes in the Ventura Basin, southern California, *J. geophys. Res.* **97,** 437–447.

Carena, S. & Moder, C., 2009. The strength of faults in the crust in the western United States, *Earth planet. Sci. Lett.,* **287,** doi:10.1016/j.epsl.2009.08.021.

Doser, I. D. & Kanamori, H., 1986. Depth of seismicity in the Imperial Valley region (1977–1983) and its relationship to heat flow, crustal structure, and the October 15, 1979, earthquake, *J. geophys. Res.,* **91,** 675–688.

Enescu, B., Hainzl, S. & Ben-Zion, Y., 2009. Correlations of seismicity patterns in Southern California with surface heat flow data, *Bull. seism. Soc. Am.,* **99**(6), 3114–3123, doi:10.1785/0120080038.

Fay, N. P., Bennett, R.A., Spinler, J.C., & Humphreys, E.D., 2008. Small-scale upper mantle convection and crustal dynamics in southern California, *Geochem. Geophys. Geosyst.,* **9,** Q08006, doi:10.1029/2008GC001988.

Hauksson, E., 2000. Crustal structure and seismicity distributions adjacent to the Pacific and north America plate boundary in southern California, *J. geophys. Res.,* **105,** 13 875–13 903.

Hauksson, E., 2010. Spatial separation of large earthquakes, aftershocks, and background seismicity: analysis of interseismic and coseismic seismicity patterns in southern California, *Pure appl. Geophys.*, **167,** doi:10.1007/s00024-010-0083-3.

Hauksson, E., & Jones, L.M., 1988. The July 1986 Oceanside ($M_L = 5.3$) earthquake sequence in the Continental Borderland, Southern California, *Bull. seism. Soc. Am.* **78,** 1885–1906.

Hutton, L. K., Woessner, J. & Hauksson, E., 2010. Seventy-seven years (1932 – 2009) of Earthquake monitoring in southern California, *Bull. seism. Soc. Am,* **100**(2); 423–446; doi:10.1785/0120090130.

Jackson, J., McKenzie, D., Priestley, K. & Emmerson, B., 2008. New views on the structure and rheology of the lithosphere, *J. Geol. Soc. Lond.,* **165,** 453–465.

Krause, D. C., 1965. Tectonics, bathymetry, and geomagnetism of the southern continental borderland west of Baja California, Mexico, *Geol. Soc. Am. Bull.,* **76**(6), 617–650; doi:10.1130/0016-7606(1965)76[617:TBAGOT]2.0.CO;2.

Lachenbruch, A. H., 1970. Crustal temperature and heat production: implications of the linear heat-flow relation, *J. geophys. Res.,* **75,** 3291–3300.

Langenheim, V. & Hauksson, E., 2001. Comparison between crustal density and velocity variations in southern California, *Geophys. Res. Lett.,* **28,** 3087–3090.

Lin, G. & Shearer, P.M. 2009. Evidence for water-filled cracks in earthquake source regions, *Geophys. Res. Lett.,* **36,** L17315, doi:10.1029/2009GL039098.

Lin, G., Shearer, P.M. & Hauksson, E., 2007. Applying a three-dimensional velocity model, waveform cross correlation, and cluster analysis to locate southern California seismicity from 1981 to 2005, *J. geophys. Res.,* **112,** B12309, doi:10.1029/2007JB004986.

Magistrale, H., 2002. Relative contributions of crustal temperature and composition to controlling the depth of earthquakes in Southern California, *Geophys. Res. Lett,* **29,** 10, 1447, doi:10.1029/2001GL014375.

Magistrale, H. & Zhou, H., 1996. Lithologic control of the depth of earthquakes in southern California, *Science,* **273,** 639–642.

Magistrale, H., Day, S., Clayton, R. W. & Graves, R., 2000. The SCEC southern California reference three-dimensional seismic velocity model version 2, *Bull. seism. Soc. Am., **90***, S65–S76.

Nakajima, J., Matsuzawa, T., Hasegawa, A. & Zhao, D., 2001a. Three dimensional structure of V_p, V_s and V_p/V_s beneath the northeastern Japan arc: implications for arc magmatism and fluids, *J. geophys. Res.,* **106,** 21 843–21 857.

Nazareth, J. J. & Hauksson, E., 2004. The Seismogenic thickness of the southern California crust, *Bull. seism. Soc. Am.,* **94,** 940–960.

Plesch, A., *et al*., 2007. Community Fault Model (CFM) for Southern California, *Bull. seism. Soc. Am.,* **97,** 1793–1802.

Sibson, R. H., 1982. Fault zone models, heat flow, and the depth distribution of earthquakes in the continental crust of the United States, *Bull. seism. Soc. Am.* **72,** 151–163.

Sibson, R. H., 1984. Roughness at the base of the seismogenic zone: contributing factors, *J. geophys. Res.*, **89,** 5791–5799.

Sibson, R.H. & Rowland, J.V., 2003. Stress, fluid pressure and structural permeability in seismogenic crust, North Island, New Zealand, *Geophys. J. Int.,* **154,** 584–594.

Takei, Y., 2002. Effect of pore geometry on V_P/V_S: from equilibrium geometry to crack, *J. geophys. Res.,* **107**(B2), 2043, doi:1029/2001JB000522.

Tanaka, A. & Ishikawa, Y., 2002. Temperature distribution and focal depth in the crust of the northeastern Japan, *Earth Planets Space,* **54,** 1109–1113.

Tape, C., Muse P., Simons, M., Dong D. & Webb, F., 2009. Multiscale estimation of GPS velocity fields, *Geophys. J. Int.,* **179,** 945–971.

Unruh, J. & Hauksson, E., 2009. Seismotectonics of an evolving intracontinental plate boundary, southeastern California, *Geol. Soc. Am. Spec. Papers,* **447,** 351–372, doi:10.1130/.90027442(61).

Vidale, J.E. & Shearer, P.M., 2006. A survey of 71 earthquake bursts across southern California: exploring the role of pore fluid pressure fluctuations and aseismic slip as drivers, *J. geophys. Res.,* **111,** B05312, doi:1029/2005JB004034.

Wessel, P. & Smith, W.H.F., 1998. New version of the generic mapping tools released, *EOS, Trans. Am. geophys. Un.,* **79,** 579, doi:10.1029/98EO00426.

Wong, I.G. & Chapman, D.S., 1990. Deep intraplate earthquakes in the Western United States and their relationship to lithospheric temperatures, *Bull. seism. Soc. Am.,* **80**(3), 589–599.

Yan, Z. & Clayton, R.W., 2007. Regional mapping of the crustal structure in southern California from receiver functions, *J. geophys. Res.,* **112,** B05311, doi:10.1029/2006JB004622.

Yang, W. & Ben-Zion, Y., 2009. Observational analysis of correlations between aftershocks productivities and regional conditions in the context of a damage rheology model, *Geophys. J. Int.* **177,** 481–490.

Zhu, L. P. & Kanamori, H., 2000. Moho depth variation in southern California from teleseismic receiver functions, *J. geophys. Res.,* **105**(B2), 2969–2980.

APPENDIX: NORMALIZING THE NUMBER OF EARTHQUAKES

The available range of geophysical variables is highly variable. For instance, low elevation topography is common while high elevation topography is rare. To account for this variability when determining if earthquakes prefer to occur within a certain range of a geophysical variable, we use the following approach to normalize the number of earthquakes per available range of each of the geophysical variables.

Where a geophysical quantity β (such as heat flow, topography, etc.) is $x \leq \beta \leq x+ \partial x$, the total number of quakes in the cells is

$$n(x)\partial x. \tag{A1}$$

The total number of cells where in which $x \leq \beta \leq x+ \partial x$

$$m(x)\partial x. \tag{A2}$$

The total number of quakes is

$$N = \int n(x)\partial x. \tag{A3}$$

The total number of cells is

$$M = \int m(x)\partial x. \tag{A4}$$

The black curve in Figs 2(c)–10(c) is $B = n(x)/N$.

The red curve in Figs 2(c)–10(c) is $R = m(x)/M$.

Then the curves marked with red data points in Figs 2(d)–10(d) are

$$\text{Ratio} = B/R = (n(x)/N)/(m(x)/M). \tag{A5}$$

Thus providing a normalized number of quakes per available range of values for each of the geophysical variables.